

Active drive towards elastic spinodals

Ayan Roychowdhury,¹ Madan Rao,¹ and Lev Truskinovsky²

¹*Simons Centre for the Study of Living Machines,*

National Centre for Biological Sciences-TIFR, Bengaluru, India 560065.

²*PMMH, CNRS-UMR 7636, PSL-ESPCI, 10 Rue Vauquelin, Paris 75005, France.*

Active renewable matter, a distinctive feature of adaptive living materials, can exhibit highly unusual mechanical responses by actively navigating the space of material parameters. In particular, it can self-drive towards elastic spinodals where the presence of inhomogeneous floppy modes, makes the matter elastically degenerate. The main effect of the implied marginality is stress localization leading in some cases to the emergence of force chains which can be actively assembled and disassembled. In this Letter we formalize the concept of spinodal states for general elastic solids and show how such extreme mechanical regimes can be actively navigated.

Active living materials, operating far from equilibrium, can manipulate the loss and recovery of elastic rigidity [1–3] through the transduction of metabolic resources [4]. Moreover, active materials often provide dynamic realizations of fragile elasticity [5], that is, such systems can marginalize their elastic response by actively modifying their energy landscape [6–10].

A prototypical context is the vast repertoire of rigidities exhibited by the active cellular cytoskeleton whose remodeling can render the cell either pliable or rigid [11]. Behind this remarkable mechanical response are the molecular motors that can either stiffen the cytoskeleton through actively generated pre-stress or fluidize it by facilitating remodeling [12].

Another striking example of the collapse of the conventional elastic response in active systems is the emergence of extreme stress and strain concentration which takes the form of force channeling – as in actomyosin ‘stress fibers’ [13] or ‘dense tethers’ during active remodelling of the extracellular matrix [14].

In this Letter, we formalize the idea of partial rigidity loss in elastic solids and identify strategies that can direct active materials towards marginal and fragile regimes. The richness of the emerging soft modes is revealed by studying inhomogeneous deformations that can be generated by internal loading in constrained environments.

The crucial insight is the elaboration of the concept of *elastic spinodals*, as opposed to the conventional thermodynamic spinodals [15]. This distinction is caused by the dominance in elastic systems of long range interactions arising from elastic compatibility induced by the gradient nature of the order parameter.

To define elastic spinodals we choose the simplest case of an isotropic linear elastic solid in 2D whose energy is $w(\boldsymbol{\epsilon}) = (\lambda/2) (\text{tr } \boldsymbol{\epsilon})^2 + \mu \text{tr } \boldsymbol{\epsilon}^2$, where $\boldsymbol{\epsilon} = (\nabla \mathbf{u} + \nabla \mathbf{u}^T)/2$ is the strain tensor, $\mathbf{u}(\mathbf{x})$ is the displacement field and λ, μ are the Lamé parameters. The corresponding stress-strain relation is $\boldsymbol{\sigma} = \mathbb{C}\boldsymbol{\epsilon}$ where $\mathbb{C}_{ijkl} = B\delta_{ij}\delta_{kl} + \mu(\delta_{ik}\delta_{jl} + \delta_{il}\delta_{jk} - \delta_{ij}\delta_{kl})$ is the isotropic fourth order (I4) stiffness tensor depending here on two physical parameters: $B = \lambda + \mu$ (bulk modulus) and μ (shear modulus).

The stability thresholds for such a solid, rep-

resenting elastic spinodals, can be found by first writing the Navier’s equilibrium equations: $\Delta \mathbf{u} + (B/\mu) \nabla(\text{div } \mathbf{u}) = 0$. After Fourier transform $\hat{\mathbf{u}}(\mathbf{q}) = (1/2\pi) \int_{\mathbb{R}^2} \mathbf{u}(\mathbf{x}) e^{-2\pi i \mathbf{x} \cdot \mathbf{q}} d\mathbf{x}$, these equations take an algebraic form $\mathbf{A}(\mathbf{q}) \hat{\mathbf{u}}(\mathbf{q}) = \mathbf{0}$, where $\mathbf{A}(\mathbf{q}) = (B + \mu) \mathbf{q} \otimes \mathbf{q} + \mu(\mathbf{I} - \mathbf{q} \otimes \mathbf{q})$ is the acoustic tensor, whose structure suggests that $B + \mu$ and μ are the two eigenvalues of the elasticity operator. The marginality condition $\det \mathbf{A}(\mathbf{q}) = 0$ is satisfied whenever either $\mu = 0$ or $B + \mu = 0$. Reaching these thresholds indicates that the Navier’s equations lose their conventional elliptic nature and signals that the character of stress propagation undergoes a fundamental change [16, 17].

The first of these two thresholds, $\mu = 0$, corresponds to the state where the material has just lost shear resistance (elastic liquid). In contrast, at the second threshold, $B + \mu = 0$, it is the resistance to longitudinal deformation that is lost (elastic aether) [18]. Such stability limits are necessarily weaker than the ones delineating thermodynamic spinodals, as the latter, see [19], deal only with homogeneous (finite dimensional) deformations. Note that the elastic regimes located between the elastic and the thermodynamic spinodals are stable only as long as the boundary is fully constrained [20].

To see how the elastic spinodals can be reached actively (while keeping the actomyosin cytoskeleton as the main example), we write the total stress $\boldsymbol{\sigma}$ (of an active meshwork) as a sum of elastic and active terms $\boldsymbol{\sigma} = \mathbb{C}^e \boldsymbol{\epsilon} + \boldsymbol{\sigma}^a$. Here \mathbb{C}^e is the elastic modulus tensor of the passive material with I4 form, and $\boldsymbol{\sigma}^a = \mathbb{A}\mathbf{M}$ is the active stress with the symmetric second order fabric tensor field $\mathbf{M}(\mathbf{x})$ representing the density distribution of active agents and encoding, for instance, a locally diffused dipolar mass anisotropy [21, 22]. The fourth order tensor \mathbb{A} is assumed to be again of I4 form with coefficients ζ and ξ , characterizing the levels of spherical and deviatoric activity, respectively.

The constitutive turnover of active elements can be incorporated into the model through the assumption that fabric anisotropy \mathbf{M} is enslaved to stress anisotropy, as the latter can, for instance, locally re-orient the cytoskeletal meshwork [23]. The simplest assumption of this type

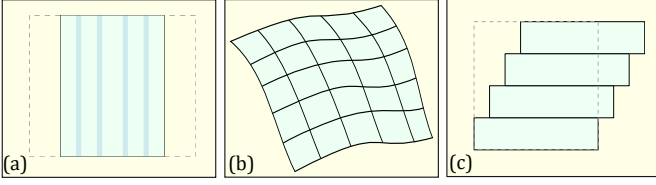


FIG. 1. Singular mechanical response on elastic spinodals: (a) elastic aether regime $B + \mu = 0$ (folding); (b) elastically stable regime $\mu > 0, B + \mu > 0$ (compatible deformation); (c) elastic liquid regime $\mu = 0$ (slipping). For the relative location of all three regimes in the space of renormalized elastic moduli (B, μ), see [19].

is $\mathbf{M}(\mathbf{x}) = \mathbf{M}_0 + \mathbb{L}\boldsymbol{\sigma}(\mathbf{x})$ [21, 22], where \mathbf{M}_0 is a constant second order tensor while the fourth order tensor \mathbb{L} is again assumed to be of I4 form, now with coefficients L_b and L_s .

Note that in the cytoskeletal setting, we are essentially postulating that the tensorial kinetic rate of binding of active crosslinkers $\mathbf{k}^b = k^b \mathbf{I}$ is balanced by a Bell-type stress dependent unbinding rate $\mathbf{k}^u \mathbf{M}$ with $\mathbf{k}^u(\boldsymbol{\sigma}) = k^u(\mathbf{I} + e^{\hat{\mathbb{L}}\boldsymbol{\sigma}})$ [24], where $\hat{\mathbb{L}}$ is again of I4 form. Under these assumptions we obtain that in the limit of small stress, $\mathbf{M}_0 = (k^b/2k^u)\mathbf{I}$ and $\mathbb{L} = -(k^b/4k^u)\hat{\mathbb{L}}$.

If we now eliminate \mathbf{M} from the stress-strain relation we obtain $\mathbb{C}\boldsymbol{\epsilon} + (\mathbb{I} - \mathbb{A}\mathbb{L})^{-1}\mathbb{A}\mathbf{M}_0$ where $\mathbb{C} := (\mathbb{I} - \mathbb{A}\mathbb{L})^{-1}\mathbb{C}^e$ is the effective (renormalized) linear elasticity tensor. In the limit of weak activity we can write the expressions for the ensuing elastic parameters explicitly: $B = B^e(1 + 4\zeta L_b)$ and $\mu = \mu^e(1 + 4\xi L_s)$.

Note that if we had assumed that the fabric tensor \mathbf{M} is regulated by the strain $\boldsymbol{\epsilon}$ (rather than the stress $\boldsymbol{\sigma}$) and postulated that $\mathbf{M} = \mathbf{M}_0 + \mathbb{K}\boldsymbol{\epsilon}$, where the tensor \mathbb{K} has the same I4 structure with parameters $K_{b,s}$, the renormalized linear elastic moduli would have been $B = B^e + 2\zeta K_b$ and $\mu = \mu^e + 2\xi K_s$. One can see that at either $L_{b,s} < 0$ or $K_{b,s} < 0$ (as in ‘catch’ bonds [9, 10, 25]), the effective moduli B and μ can potentially reach the elastic spinodal limits when the activity levels, characterized by the coefficients ζ or ξ , are sufficiently high. Note that while the synthesis of inanimate materials with $B + \mu = 0$ remains highly challenging, not in the least due to its peculiar ‘infinitely auxetic’ response, e.g. [26], such designs have been already proposed and implemented for metamaterials with $\mu = 0$ [27].

To clarify the physical meaning of the elastic spinodal limits, we first observe that in the case of elastic liquid ($\mu = 0$) the soft modes are solenoidal ($\text{div } \mathbf{u} = 0$), while in the case of elastic aether ($B + \mu = 0$), they are irrotational ($\text{curl } \mathbf{u} = \mathbf{0}$). Furthermore, due to the scale-free nature of continuum elasticity, at these thresholds all wavelengths become unstable simultaneously [28]. Interestingly, the equilibrium mechanical response at elastic spinodals becomes isostatic [29] – thus for the elastic liquid the deviatoric stress must be necessarily equal to

zero, $\boldsymbol{\sigma} - (1/2)\text{tr}[\boldsymbol{\sigma}]\mathbf{I} = \mathbf{0}$, while for elastic aether it is the determinant of the stress tensor that must necessarily vanish, $\det[\boldsymbol{\sigma}] = 0$.

To reveal the inherently singular nature of these isostatic responses, it is convenient to turn to the classical Airy stress function χ which parametrizes equilibrium stress fields so that $\sigma_{xx} = \partial_{yy}^2\chi$, $\sigma_{yy} = \partial_{xx}^2\chi$, $\sigma_{xy} = -\partial_{xy}^2\chi$. In terms of χ , the remaining equilibrium equations for elastic liquids ($\mu = 0$) take the form of two *hyperbolic* equations $\partial_{xx}^2\chi - \partial_{yy}^2\chi = 0$ and $\partial_{xy}^2\chi = 0$, while for elastic aether ($B + \mu = 0$), we similarly obtain a single *degenerate-elliptic* Monge-Ampère equation $\partial_{xx}^2\chi \partial_{yy}^2\chi - (\partial_{xy}^2\chi)^2 = 0$. In both cases the equilibrium problem admits (static) shock wave type solutions with discontinuous gradients of the Airy function χ indicating the presence of displacement jumps $[\mathbf{u}] \neq 0$ [30, 31]. For the elastic liquid such jumps reflect the formation of slip lines, while in the case of elastic aether they can describe self penetration, see Fig. 1(b). In other words, on elastic spinodals the graph of $\chi(\mathbf{x})$ may develop sharp folds, while outside, where elasticity remains non-degenerate and elastic compatibility holds, the function χ is necessarily smooth.

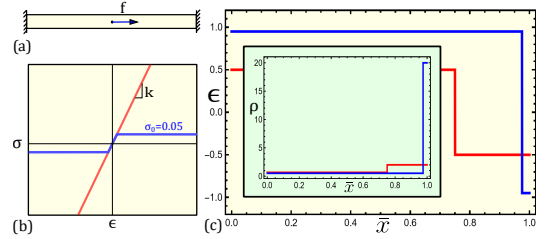


FIG. 2. Strain localization in a loaded elastic bar (a) whose response (b) is approaching the elastic spinodal limit. In (c) we show the strain $\epsilon = du/dx$, where $u(x)$ is the displacement field, in the deformed coordinates $\tilde{x} = x + u(x)$; the inset shows the density distribution $\rho(x) = 1/(1 + \epsilon(x))$. All variables are dimensionless, $k = 1$ and $f = 1$.

As an elementary illustration of strain localization at elastic spinodals, consider a 1D bar subjected to a body force f applied at the center, with its ends fixed, see Fig. 2 (a). Suppose that the stress-strain relation for the material of the bar has a linear elastic range with modulus k which ends with stress saturation in both tension and compression at $\pm\sigma_0$, see Fig. 2 (b). When the elastic spinodal limit is approached at $\sigma_0 \rightarrow 0$, mass density singularly localizes near one of the boundaries while the rest of the bar decompresses into a void, see Fig. 2(c). This example illustrates a tendency towards fraying (fragmentation) at the elastic aether limit where under internal loading a homogeneous state can turn into a collection of sparsely distributed dense fibers.

As we have already mentioned, actomyosin cytoskeleton represents perhaps the most striking realization of such self-induced stress concentrators which can take the

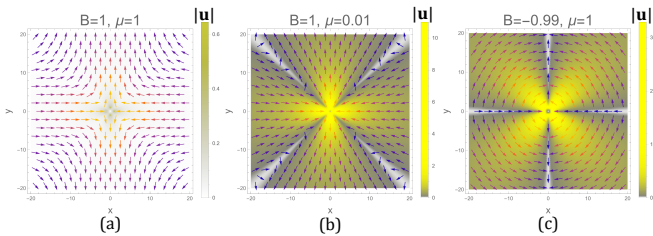


FIG. 3. Elastic response to a force quadrupole placed at the origin: (a) displacement field in a non-degenerate regime; (b) close to elastic liquid limit; (c) close to aether limit. Notice the formation of the localized singularities of the displacement field in the regimes (b) and (c).

form of transitory, assembled and disassembled force-carrying ‘frames’ [13, 32]. In the context of cytoskeletal mechanics, the microscopic accessibility of the elastically degenerate regimes can be attributed to the microbuckling [33], the loss of crosslinkers, resulting in relative sliding of the semiflexible actin filaments [34], to micro-wrinkling [35] and can also be linked to the stretching-to-bending transition [36].

The tendency towards the formation of displacement discontinuities in elastic spinodal regimes can be most easily seen by examining the structure of the corresponding Green’s functions [37]. For instance, by computing the Fourier image of the inverse acoustic tensor $\hat{G}_{ij}(q_x, q_y) = [B q_i q_j + \mu q_k q_k \delta_{ij}]^{-1}$, we can construct the displacement fields generated by a pure shear quadrupole, clearly showing the development of jumps as the elastic aether or elastic liquid limits are approached, see Fig. 3(b,c). Note that in the case of elastic aether, along the singular lines material can both ‘fold’ under uniaxial compression (as in membrane wrinkling [38]), and ‘unfold’ under uniaxial tension (as in the case of granular media [39]). For elastic liquids similar singular solutions with localized displacement discontinuities are usually discussed in the dynamic framework as weak solutions of Euler equations containing vortex sheets and other singular structures, e.g. [40].

Note that in living cells, the constraint on the boundaries required for reaching the elastic spinodals can be ensured by confluent tissues. Such constraints are also effectively operative in cells adhered on micro-patterned substrates [13] where the emergence of cell spanning cytoskeletal ‘force chains’ is known to be linked to the anchoring at the cell boundaries (through focal adhesions [41]). Since an arbitrary distribution of the anchoring sites would not in general be compatible with the equilibrium structure of the force chain network, a dynamic reorganization of the anchoring configurations and a concomitant reconfiguration of the force chains in the bulk, could be expected to characterize the inherently fragile mechanical response of a living cell [10, 42, 43] In the case of elastic aether the implied ‘holographic’

bulk-boundary correspondence would originate from the fact that its energy density is a null-Lagrangian [44] $\int_{\Omega} w(\epsilon) dA = \int_{\partial\Omega} \tau_a(\mathbf{u}, \nabla \mathbf{u}, \boldsymbol{\nu}) dx$ where $\tau_a(\mathbf{u}, \nabla \mathbf{u}, \boldsymbol{\nu}) = -\mu e_{ik} e_{jl} \partial_i u_j u_k \nu_l$ is a ‘live load’ type surface energy, e_{ij} is the Levi-Civita symbol, and $\boldsymbol{\nu}$ denotes the unit normal to the boundary.

It is instructive to compare elastic spinodals with the classical thermodynamic spinodals. While the former is signalled by the emergence of zero eigenvalues of an infinite dimensional operator, the latter is associated with the appearance of zero eigenvalues of a finite dimensional matrix. Thermodynamic spinodals delineate the boundaries of the domain of convexity of elastic energy density in the strain space and mark states where the positive definiteness of the stiffness tensor is lost [19]. In the case of linear isotropic solid the thermodynamic spinodals are either $B = 0$ or $\mu = 0$. In the space of the eigenvalues of the strain tensor (ϵ_1, ϵ_2) both of these degeneracies appear as a transformation of a single minimum of the elastic energy at $\epsilon_1 = \epsilon_2 = 0$ into zero energy valleys, representing continuously distributed minima: zero dilatation valley $\epsilon_1 + \epsilon_2 = 0$ in the case $B = 0$ (unimodal material) and zero shear valley $\epsilon_1 - \epsilon_2 = 0$ in the case $\mu = 0$ (bimodal material) [45]. Thermodynamic spinodals have been successfully reached by meta-material constructions [46], while for the cytoskeleton context, they may be relevant to suspended cells [47].

Since the elastic liquid regime $\mu = 0$ corresponds to both, an elastic and a thermodynamic spinodal, it is natural to show the specificity of the latter by considering another thermodynamic stability limit $B = 0$. The peculiarity of this regime is that the two components of the displacement field (u_x, u_y) are harmonic functions and that the deformation gradient $\nabla \mathbf{u}$ is necessarily a product of dilatation and rotation [19]. The corresponding non-affine floppy modes are angle preserving and therefore conformal [48]. The stress in such a ‘conformal’ solid is necessarily trace free, $\text{tr}[\boldsymbol{\sigma}] = 0$, which makes the equilibrium problem $\text{div } \boldsymbol{\sigma} = \mathbf{0}$ again statically determinate (isostatic) [49]. The resulting elastic system is unstable under action of boundary forces and any unconstrained segment of the boundary can be expected to undergo a surface instability, as the condition $B = 0$ also marks the failure of the corresponding surface stability condition [20, 50].

So far our analysis has been limited to a linear elastic response. We now show that in a nonlinear setting, the elastic spinodal can coexist with thermodynamic critical points.

Note first that if the equilibrium kinetic model, linking the fields \mathbf{M} and $\boldsymbol{\epsilon}$, is kept in its original nonlinear form, the effective stress-strain relation can become nonmonotone. Thus, if in the simplest 1D scalar model, the condition of chemical equilibrium $m_0 = (1 + e^{\hat{L}\boldsymbol{\epsilon}}) m$ is inverted (leaving only the first nonlinear term in the small strain expansion) and then substituted into the expression for

stress, we obtain a cubic renormalized stress-strain relation: $\sigma(\epsilon) = m_0\zeta/2 + (\mu - m_0\zeta\hat{L}/4)\epsilon + (m_0\zeta\hat{L}^3/48)\epsilon^3$ [9, 10]. Then at sufficiently large $\hat{L} > 0$ the corresponding quartic effective elastic energy has a double-well form and the unstable homogeneous reference state can be expected to decompose into contracted ($\epsilon < 0$) and stretched ($\epsilon > 0$) domains.

In 2D tensorial setting, a similar quartic effective elastic energy density can be written in the form $w(\epsilon_1, \epsilon_2) = \frac{B}{2}(\epsilon_1 + \epsilon_2)^2 + \frac{\mu}{2}(\epsilon_1 - \epsilon_2)^2 + \frac{B'}{4}(\epsilon_1 + \epsilon_2)^4 + \frac{\mu'}{4}(\epsilon_1 - \epsilon_2)^4$, where $B' > 0$ and $\mu' > 0$ are the third order elastic moduli at the reference state. As we have seen, activity can renormalize the second order reference moduli towards the values $\mu = 0$ and $B = -\mu$, but in the nonlinear setting both these thresholds can be crossed because even if the reference state is destabilized, the new energy minima will emerge.

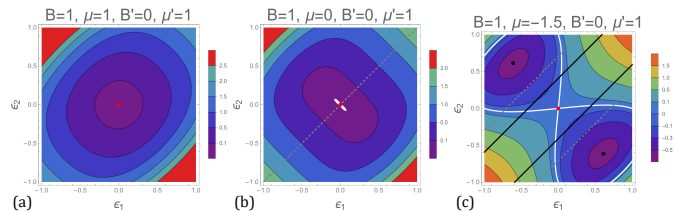


FIG. 4. Evolution of the prototypical energy landscape $w(\epsilon_1, \epsilon_2)$ as the configuration at the origin approaches and passes the elastic liquid limit: (a) non-degenerate solid; (b) elastic liquid; (c) post-liquid unstable. Elastic spinodals are shown by solid black lines, while thermodynamic spinodals are shown by dotted gray lines. White lines mark zero energy valleys.

In particular, passing the elastic liquid threshold at activity level $\xi = -\mu^e/(2K_s)$ produces two new energy minima along the deviatoric axis, $\epsilon_1 - \epsilon_2$, while along the perpendicular hydrostatic tensorial direction $\epsilon_1 + \epsilon_2$ the energy remains convex, see Fig. 4. Similarly, passing the elastic aether threshold at $\zeta = -(B^e + \mu^e)/2K_b$ generates two new minima along the $\epsilon_1 + \epsilon_2$ tensorial direction while along the $\epsilon_1 - \epsilon_2$ direction the convexity of the energy is preserved, see Fig. 5.

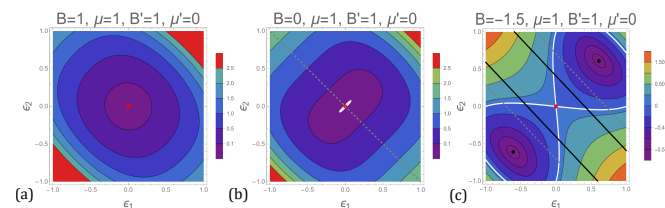


FIG. 5. Same as in Fig. 4 but now with the configuration at the origin approaching and passing the elastic aether limit: (a) non-degenerate solid; (b) thermodynamic spinodal; (c) post-aether, unstable. At the elastic spinodal ($B + \mu = 0$) regime the two black lines collapse into one passing through the origin.

Note that in the *post-liquid* regimes with $\mu \lesssim 0$, the two apparently isolated new nonlinear energy minima, shown in Fig. 4, are in fact connected (and are therefore degenerate) as they represent a continuous family of pure shears related through rigid rotations. The corresponding energy minimizing mixtures should resemble microstructures encountered in nematic elastomers [51]. Interestingly, under some additional assumptions, a pronounced force channeling has been observed numerically in such nonlinear elastic models [14, 52]. In the *post-aether* regimes with $B \lesssim -\mu$, the new nonlinear energy minima, shown in Fig. 5, are indeed isolated and represent configurations with different densities.

In both cases discussed above, crossing thermodynamic spinodal thresholds of the linearized model, produces activity-induced second order phase transitions. In this sense thermodynamic spinodals transform into classical critical points. On the other hand, crossing elastic spinodal thresholds of the linearized model produces elastic spinodals of the nonlinear problem [19], see black lines in Fig. 4 and Fig. 5. The emerging new elastically degenerate regimes can be reached both passively [53] and actively [54].

So far, the nonequilibrium nature of the drive towards elastic spinodals was concealed behind the fact that active and passive stresses could be represented together by an effective quasi-elastic energy density [9, 10]. A simple zero dimensional model can illustrate the fact that behind the ‘renormalization’ of the elastic energy is a non-equilibrium energy reservoir [6–8]. Consider an overdamped ratchet-type stochastic system described by the Langevin equation $\dot{x} = -\partial_x G + \sqrt{2D}\eta(t)$, where $\eta(t)$ is a standard white noise with unit variance, D is a measure of temperature and $G(x, t) = V(x, t) + k(x - z)^2/2$ is the energy which includes a confining (time-dependent) nonconvex potential. To represent active rocking we write $V(x, t) = V(x) - xf(t)$, where $V(x) = (1/2)(x^2 - 0.1)(x^2 - 0.5)^2$ and $f(t) = A(-1)^{n(t)}$, with $n(t) = \lfloor 2t/\tau \rfloor$, is the external force representing correlated (active) noise with zero average. In addition, the configuration of this non-equilibrium system is probed externally through a spring with stiffness k and a control parameter z , see the inset in Fig. 6(a).

The effective force exerted on the spring can be found by averaging the response over ensemble and over time, $T(z) = k[z - \lim_{t \rightarrow \infty} (1/t) \int_0^t \int_{-\infty}^{\infty} xp(x, t) dx dt]$. To find the probability distribution $p(x, t)$ one must solve the corresponding Fokker-Planck equation $\partial_t p = \partial_x [p \partial_x G + D \partial_x p]$ and the ensuing potential $F(z) = \int^z T(s) ds$ would then play the role of an effective (renormalized) elastic energy. This problem can be solved analytically in the adiabatic approximation [19, 55] and the typical effective energy is shown in Fig. 6. With growing activity level (increasing A), the energy minimum at $z = 0$ first flattens and then turns into a maximum as the

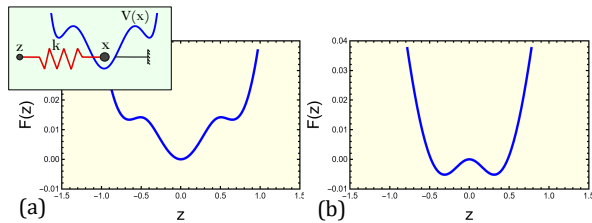


FIG. 6. The effective potential $F(z)$ at different levels of activity: (a) $A = 0$ and (b) $A = 0.4$, with $D = 0.01$.

reference state passes beyond the state of zero rigidity.

To conclude, our analysis reveals the multifaceted nature of the thresholds of marginal elastic stability in solids. At these thresholds non-affine deformations can proceed at zero energy cost which opens the possibility for force channeling. An explicit realization of such exotic mechanical states can be expected in active cytoskeleton which possesses all the necessary machinery to navigate to and from the elastic spinodals while taking advantage of the associated fragile responses. While in isotropic solids we found only two elastic spinodal regimes, other types of fragilized soft modes would exist in anisotropic [56] and odd elastic systems [57].

[1] P. M. Chaikin and T. C. Lubensky, *Principles of Condensed Matter Physics*, Cambridge University Press (1995).

[2] S. Alexander, *Amorphous solids: Their structure, lattice dynamics and elasticity*, Physics Reports **296**, 65–236 (1998).

[3] C. P. Goodrich, A. J. Liu and S. R. Nagel, *The Principle of Independent Bond-Level Response: Tuning by Pruning to Exploit Disorder for Global Behavior*, Physical Review Letters **114**, 225501 (2015).

[4] R. J. Hawkins and T. B. Liverpool, *Stress Reorganisation and Response in Active Solids*, Physical Review Letters **113**, 028102 (2014).

[5] M. E. Cates, J. P. Wittmer, J. -P. Bouchaud and P. Claudin, *Jamming, force chains, and fragile matter*, Physical Review Letters **81**, 1841–1844 (1998).

[6] R. Sheshka, P. Recho and L. Truskinovsky, *Rigidity generation by nonthermal fluctuations*, Physical Review E **93**, 052604 (2016).

[7] A. Maitra and R. Voituriez, *Enhanced Orientational Ordering Induced by an Active yet Isotropic Bath*, Physical Review Letters **124**, 048003 (2020).

[8] A. Behera, M. Rao, S. Sastry and S. Vaikuntanathan, *Enhanced Associative Memory, Classification, and Learning with Active Dynamics*, Physical Review X **13**, 041043 (2023).

[9] D. S. Banerjee, A. Munjal, T. Lecuit and M. Rao, *Actomyosin pulsation and flows in an active elastomer with turnover and network remodeling*, Nature Communications **8**, 1121 (2017).

[10] A. Roychowdhury, S. Dasgupta and M. Rao, *Emergence of Tension Chains and Active Force Patterning,*

arXiv:2206.06770.

[11] S. Banerjee, M. L. Gardel and U. S. Schwarz, *The actin cytoskeleton as an active adaptive material*, Annual Review of Condensed Matter Physics **11**, 421–439 (2020).

[12] W. Xi, T. B. Saw, D. Delacour, C. T. Lim and B. Ladoux, *Material approaches to active tissue mechanics*, Nature Reviews Materials **4**, 23–44 (2019).

[13] T. Vignaud, C. Copos, C. Leterrier, M. Toro-Nahuelpan, Q. Tseng, J. Mahamid, L. Blanchoin, A. Mogilner, M. Théry and L. Kurzawa, *Stress fibres are embedded in a contractile cortical network*, Nature Materials **20**, 410–420 (2021).

[14] G. Grekas, M. Proestaki, P. Rosakis, J. Notbohm, C. Makridakis and G. Ravichandran, *Cells exploit a phase transition to mechanically remodel the fibrous extracellular matrix*. Journal of Royal Society Interface **18** 20200823 (2021).

[15] T. Chou and D. R. Nelson, *Dislocation-mediated melting near isostructural critical points*, Physical Review E **53**, 2560 (1996).

[16] J. K. Knowles and E. Sternberg, *On the failure of ellipticity and the emergence of discontinuous deformation gradients in plane finite elastostatics*, Journal of Elasticity, **8**, 329–379 (1978).

[17] R. Lakes, and K.W. Wojciechowski, *Negative compressibility, negative Poisson's ratio, and stability*, Physica status solidi (b), **245**, 545 (2008).

[18] J. Ericksen and R. Toupin, *Implications of Hadamard's conditions for elastic stability with respect to uniqueness theorems*, Canadian Journal of Mathematics, University of Toronto Press **8**, 432–436 (1956).

[19] See Supplemental Material at [URL will be inserted by publisher] for the details of the computation of thermodynamic spinodals, for the analysis of the nonlinear model and for the explicit formulas for the probability distribution in the adiabatic limit.

[20] M. Šilhavý, *The Mechanics and Thermodynamics of Continuous Media*, Springer-Verlag (1997).

[21] K. D. Irvine and B. I. Shraiman, *Mechanical control of growth: ideas, facts and challenges*, Development **144**, 4238–4248 (2017).

[22] A. Iorati-Uba, T. B. Liverpool and S. Henkes, *Mechano-chemical active feedback generates convergence extension in epithelial tissue*, Physical Review Letters **131**, 238301 (2023).

[23] W. Mirza, M. De Corato, M. Pensalfini, G. Vilanova, A. Torres-Sánchez and M. Arroyo, *Theory of active self-organisation of dense nematic structures in actin gels*, arXiv preprint arXiv:2306.15352 (2023).

[24] S. S. M. Konda, J. N. Brantley, C. W. Bielawski and D. E. Makarov, *Chemical reactions modulated by mechanical stress: extended Bell theory*, The Journal of Chemical Physics **135**, 164103 (2011).

[25] M. Kovács, K. Thirumurugan, P. J. Knight, and J. R. Sellers, *Load-dependent mechanism of nonmuscle myosin 2*, Proceedings of the National Academy of Sciences **104**, 9994–9999 (2007).

[26] M. Briane and G. A. Francfort, *A Two-Dimensional Labile Aether Through Homogenization*, Communications in Mathematical Physics **367**, 599–628 (2019).

[27] A. Cherkaev, M. Kadic, G. W. Milton and M. Wegener, *Pentamode materials: From underwater cloaking to cushioned sneakers*, SIAM News, **52**, 1–2 (2019).

[28] S. G. Mikhailin, *The spectrum of a family of operators in*

- the theory of elasticity*, Russian Mathematical Surveys **28**, 45–88 (1973).
- [29] R. Blumenfeld, *Isostaticity and Controlled Force Transmission in the Cytoskeleton: A Model Awaiting Experimental Evidence*, Biophysical Journal **91**, 1970–1983 (2006).
- [30] L. Caffarelli, L. Nirenberg and J. Spruck, *The Dirichlet Problem for the Degenerate Monge-Ampère Equation*, Revista Matemática Iberoamericana **2**, 19–27 (1986).
- [31] M. Angelillo, E. Babilio and A. Fortunato, *Singular stress fields for masonry-like vaults*, Continuum Mechanics and Thermodynamics **25**, 423–441 (2013).
- [32] D. E. Ingber, N. Wang and D. Stamenović, *Tensegrity, cellular biophysics, and the mechanics of living systems*, Reports on Progress in Physics **77**, 046603 (2014).
- [33] P. Ronceray, C. P. Boedersz and M. Lenz, *Fiber networks amplify active stress*, Proceedings of the National Academy of Sciences **113**, 2827–2832 (2016).
- [34] M. P. Murrell and M. L. Gardel, *F-actin buckling coordinates contractility and severing in a biomimetic actomyosin cortex*, Proceedings of the National Academy of Sciences **109**, 20820–20825 (2012).
- [35] P. Müller and J. Kierfeld, *Wrinkling of random and regular semiflexible polymer networks*, Physical Review Letters **112**, 094303 (2014).
- [36] O. U. Salman, G. Vitale and L. Truskinovsky, *Continuum theory of bending-to-stretching transition*, Physical Review E **100**, 051001 (2019).
- [37] D. Bigoni and D. Capuani, *Green’s function for incremental nonlinear elasticity: shear bands and boundary integral formulation*, Journal of the Mechanics and Physics of Solids **50**, 471–500 (2002).
- [38] A. C. Pipkin, *The relaxed energy density for isotropic elastic membranes*, IMA Journal of Applied Mathematics **36**, 85–99 (1986).
- [39] R. P. Behringer and B. Chakraborty, *The physics of jamming for granular materials: a review*, Reports on Progress in Physics **82**, 012601 (2018).
- [40] A. J. Chorin, *Vorticity and Turbulence (Vol. 103)*, Springer Science and Business Media (2013).
- [41] I. L. Novak, B. M. Slepchenko, A. Mogilner and L. M. Loew, *Cooperativity between cell contractility and adhesion*, Physical Review Letters **93**, 268109 (2004).
- [42] C. Floyd, H. Levine, C. Jarzynski and G. A. Papoian, *Understanding cytoskeletal avalanches using mechanical stability analysis*, Proceedings of the National Academy of Sciences **118**, e2110239118 (2021).
- [43] J.-P. Bouchaud, P. Claudin, M.E. Cates, J.P. Wittmer, *Models of stress propagation in granular media*, in Physics of Dry Granular Media, H.J. Herrmann, J.P. Hovi and S. Luding (Eds.), NATO ASI, 97–121 (1997).
- [44] M. R. Lancia, G. V. Caffarelli and P. Podio-Guidugli, *Null Lagrangians in linear elasticity*, Mathematical Models and Methods in Applied Sciences **5**, 415–42 (1995).
- [45] G. W. Milton and A. V. Cherkaev, *Which elasticity tensors are realisable?*, Journal of Engineering Materials and Technology **117**, 483–493 (1995).
- [46] A. Ninarello, J. Ruiz-Franco and E. Zaccarelli, *Onset of criticality in hyper-axetic polymer networks*, Nature Communications **13**, 527 (2022).
- [47] J. M. Maloney, D. Nikova, F. Lautenschläger E. Clarke, R. Langer, J. Guck and K. J. Van Vliet, *Mesenchymal Stem Cell Mechanics from the Attached to the Suspended State*, Biophysical Journal **99**, 2479–2487 (2010).
- [48] M. Czajkowski, C. Coulais, M. van Hecke and D. Z. Rocklin, *Conformal elasticity of mechanism-based metamaterials*, Nature Communications **13**, 211 (2022).
- [49] P. Broedersz, X. Mao, T. C. Lubensky and F. C. MacKintosh, *Criticality and Isostaticity in Fibre Networks*, Nature Physics **7**, 983–988 (2011).
- [50] H. C. Simpson and S. J. Spector, *On the failure of the complementing condition and non-uniqueness in linear elastostatics*, Journal of Elasticity **15**, 229–231 (1985).
- [51] S. Conti, A. DeSimone and G. Dolzmann, *Semisoft elasticity and director reorientation in stretched sheets of nematic elastomers*, Physical Review E **66**, 061710 (2002).
- [52] S. A. Silling, *Numerical studies of loss of ellipticity near singularities in an elastic material*, Journal of Elasticity **19**, 213–239 (1988).
- [53] P. Rosakis, *Ellipticity and deformations with discontinuous gradients in finite elastostatics*, Archive for Rational Mechanics and Analysis **109**, 1–37, (1990).
- [54] M. F. Staddon, A. Hernandez, M. J. Bowick, M. Moshe and M. C. Marchetti, *The role of non-affine deformations in the elastic behavior of the cellular vertex model*, Soft Matter **19**, 3080–3091 (2023).
- [55] M. O. Magnasco, *Forced thermal ratchets*, Physical Review Letters **71**, 1477 (1993).
- [56] D. Bigoni and P. A. Gougiotis, *Folding and Faulting of an Elastic Continuum*, Proceedings of the Royal Society of London A **472**, 20160018 (2016).
- [57] C. Scheibner, A. Souslov, D. Banerjee, P. Surówka, W. T. M. Irvine and V. Vitelli, *Odd Elasticity*, Nature Physics **16**, 475–480 (2020).

Active drive towards elastic spinodals: Supplementary Material

Ayan Roychowdhury,¹ Madan Rao,¹ and Lev Truskinovsky²

¹*Simons Centre for the Study of Living Machines,*

National Centre for Biological Sciences-TIFR, Bengaluru, India 560065.

²*PMMH, CNRS-UMR 7636, PSL-ESPCI, 10 Rue Vauquelin, Paris 75005, France.*

1. THERMODYNAMIC SPINODALS IN LINEAR ELASTICITY

We recall that for 2D isotropic materials reaching thermodynamic spinodal means the loss of convexity of the (activity renormalized) effective energy density

$$w(\epsilon_1, \epsilon_2) = B(\epsilon_1 + \epsilon_2)^2/2 + \mu(\epsilon_1 - \epsilon_2)^2/2, \quad (1)$$

written here in terms of principal strains (ϵ_1, ϵ_2) . Convexity in this setting is equivalent to the positive definiteness of the effective elastic stiffness tensor. Note that in the analysis of positive definiteness the constraint of strain compatibility is irrelevant since only homogeneous deformation are effectively taken into account.

From (1) it is clear that the resulting constraints on the moduli are $B > 0$ and $\mu > 0$. They ensure that the elastic body is stable independently of the type of the boundary conditions and, in this sense, are sufficient but not necessary for elastic stability.

To identify the floppy modes activated at the thresholds $B = 0$ and $\mu = 0$ we recall that for isotropic materials in 2D the fourth order elastic stiffness tensor \mathbb{C} can be represented as a 3×3 matrix with eigenvalues $2B$, 2μ and 2μ . Hence, at $\mu = 0$ there are two degenerate eigenvalues while at $B = 0$ there is one. It is easy to see that at the elastic fluid threshold $\mu = 0$ two shear modes soften while at the threshold $B = 0$ a single dilatation mode becomes floppy.

To understand better the less conventional threshold $B = 0$, we observe that in such a material purely dilatational deformations with $\epsilon_{xx} - \epsilon_{yy} = 0$ and $\epsilon_{xy} = 0$ are energy free. If we express these conditions in terms of displacements, we obtain $u_{x,x} = u_{y,y}$ and $u_{x,y} = -u_{y,x}$. Then

$$\nabla \mathbf{u} = \begin{pmatrix} u_{y,y} & -u_{y,x} \\ u_{y,x} & u_{y,y} \end{pmatrix} = \mathbf{R}\mathbf{U} \quad (2)$$

where $\mathbf{U} = \sqrt{a^2 + b^2}\mathbf{I}$ is a pure dilatation with $a = u_{y,y}$, $b = u_{y,x}$, and \mathbf{R} is a rotation by angle $\tan^{-1}(b/a)$. Such (soft) displacement fields are angle preserving and therefore the material with $B = 0$ is known as conformal.

While the equations of elasticity remain elliptic when the conformal threshold $B = 0$ is reached, the elastic body becomes unstable on the unconstrained part of the boundary due to the failure of the ‘complementing condition’ which marks the effective ‘loss of ellipticity on the boundary’ [1]. This means, for instance, that for a solid body with $B = 0$ the traction free boundary is always unstable against surface wrinkling of the

form $\mathbf{u}(\mathbf{x}) = \text{Re}[z(s)e^{i\mathbf{q}\cdot\mathbf{x}}]$, where \mathbf{q} is an arbitrary wave vector describing lateral oscillations and the function $z(s) = \mu(iq\nu + \mathbf{q})e^{-qs}$ describing the decay away from the free surface is exponential. Here \mathbf{x} is the surface coordinate and s is the coordinate perpendicular to the free surface with normal ν , see [2] for more details.

It is instructive to illustrate the degeneracies of the energy landscape associated with these two thermodynamic spinodal regimes. In view of isotropy, it is again convenient to use the space of principal strains (ϵ_1, ϵ_2) . Since we are in the linear elastic framework, the implied degeneracy always takes the form of a transformation of a single minimum of the quadratic elastic energy at $\epsilon_1 = \epsilon_2 = 0$, see 1(a), into the zero energy ‘valleys’ representing continuously degenerate minima: zero dilatation valley $\epsilon_1 + \epsilon_2 = 0$ in the case of an elastic fluid and zero shear valley $\epsilon_1 - \epsilon_2 = 0$ in the case of dilatation-insensitive solid, see Fig. 1(c,e). In Fig. 1(d) we show for comparison the case of an *elastic spinodal* (aether) where the ‘thermodynamically neutral’ valleys are replaced by ‘thermodynamically unstable’ soft directions.

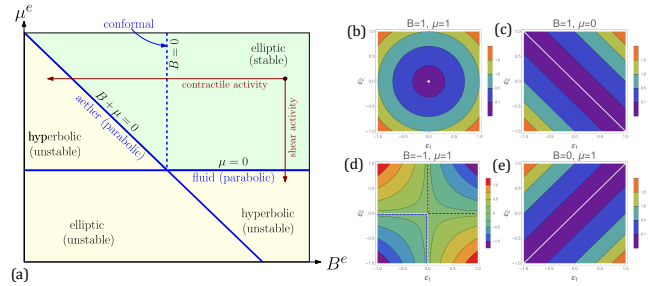


FIG. 1. (a) Regime diagram in the space of elastic moduli for the classical isotropic linear elastic solid. (b-e) Contours of the linear elastic strain energy density $w(\epsilon_1, \epsilon_2)$ for different B and μ ; white line indicates zero ‘valleys’. In (b) we see a single strain energy minimum. It transforms into a continuous distribution of minima in the thermodynamic spinodal regimes: (c) elastic fluid and (e) conformal material. In (d), we show the two soft mode branches of elastic aether $\det[\epsilon] = 0$: no compression aether: $\text{tr}[\epsilon] > 0$ (red dotted line) and no tension aether: $\text{tr}[\epsilon] < 0$ (blue dotted line).

2. THERMODYNAMIC AND ELASTIC SPINODALS IN A PHYSICALLY NONLINEAR MODEL

Activity introduces weak nonlinearity in the elastic material, resulting in the effective energy density

$$w(\boldsymbol{\epsilon}) = (B/2)\epsilon_{mm}\epsilon_{nn} + \mu\tilde{\epsilon}_{mn}\tilde{\epsilon}_{mn} + (B'/4)\epsilon_{mm}\epsilon_{nn}\epsilon_{pp}\epsilon_{qq} + \mu'\tilde{\epsilon}_{mn}\tilde{\epsilon}_{mn}\tilde{\epsilon}_{pq}\tilde{\epsilon}_{pq}. \quad (3)$$

Here $\epsilon_{mn} := (u_{m,n} + u_{n,m})/2$ is the linearized strain, ϵ_{mm} is its trace and $\tilde{\epsilon}_{mn} := \epsilon_{mn} - (\epsilon_{kk})/2\delta_{mn}$ is its deviatoric part; in addition to the standard activity renormalized linear elastic moduli B and μ , we consider here the activity induced third order moduli B' and μ' . We also use an index free notation $\boldsymbol{\epsilon} = \|\epsilon_{mn}\|$. The associated tangential stiffness tensor takes the form

$$C_{ijkl}(\boldsymbol{\epsilon}) := \partial^2 w / \partial \epsilon_{ij} \partial \epsilon_{kl} = B\delta_{ij}\delta_{kl} + \mu(\delta_{ik}\delta_{jl} + \delta_{il}\delta_{jk} - \delta_{ij}\delta_{kl}) + 3B'(\epsilon_{mm})^2\delta_{ij}\delta_{kl} + 2\mu'\tilde{\epsilon}_{pq}\tilde{\epsilon}_{pq}(\delta_{ik}\delta_{jl} + \delta_{il}\delta_{jk} - \delta_{ij}\delta_{kl}) + 8\mu'\tilde{\epsilon}_{ij}\tilde{\epsilon}_{kl}. \quad (4)$$

Thermodynamic spinodals. To locate the thermodynamic spinodals we need to determine the configurations where the effective elastic energy (3) loses convexity. Consider a small affine deformation characterized by the second order symmetric tensor $\mathbf{A} = \|a_{ij}\|$ superimposed on an arbitrary local state with a strain $\boldsymbol{\epsilon}$. The conditions of positive definiteness of the tangential stiffness tensor (depending parametrically on $\boldsymbol{\epsilon}$), can be expressed in terms of the eigenvalues of the quadratic form

$$\begin{aligned} \mathbf{CA} \cdot \mathbf{A} &= B(\text{tr } \mathbf{A})^2 + \mu\left(2|\mathbf{A}|^2 - (\text{tr } \mathbf{A})^2\right) \\ &\quad + 3B'(\text{tr } \boldsymbol{\epsilon})^2(\text{tr } \mathbf{A})^2 \\ &\quad + 2\mu'|\tilde{\boldsymbol{\epsilon}}|^2\left(2|\mathbf{A}|^2 - (\text{tr } \mathbf{A})^2\right) + 8\mu'(\tilde{\boldsymbol{\epsilon}} \cdot \mathbf{A})^2. \end{aligned} \quad (5)$$

Choosing \mathbf{A} to be spherical, $\mathbf{A} = A\mathbf{I}$, we obtain

$$\mathbf{CA} \cdot \mathbf{A} = 16\left(B + 3B'(\epsilon_1 + \epsilon_2)^2\right)A^2, \quad (6)$$

while choosing \mathbf{A} to be deviatoric, we get

$$0 \leq \mathbf{CA} \cdot \mathbf{A} \leq 2\left(\mu + 3\mu'(\epsilon_1 - \epsilon_2)^2\right)|\mathbf{A}|^2, \quad (7)$$

where we used the Cauchy-Schwarz inequality to obtain the upper bound and introduced $\epsilon_{1,2}$, the principal strains. If the strain state $\boldsymbol{\epsilon}$ lies on the thermodynamic spinodal, the right hand sides of either (6) or (7) must vanish. Therefore, in the space $\epsilon_{1,2}$, the thermodynamic spinodals are described by the two equations

$$B + 3B'(\epsilon_1 + \epsilon_2)^2 = 0, \quad (8a)$$

$$\mu + 3\mu'(\epsilon_1 - \epsilon_2)^2 = 0. \quad (8b)$$

Elastic spinodals. We begin by computing the acoustic tensor at the homogeneous state $\boldsymbol{\epsilon}$. Using the orthonormal basis $(\mathbf{q} \otimes \mathbf{q}, \mathbf{q}_\perp \otimes \mathbf{q}_\perp)$, formed by the Fourier space wave vector \mathbf{q} and its orthogonal complement \mathbf{q}_\perp , we obtain:

$$\begin{aligned} \mathbf{Q}(\boldsymbol{\epsilon}; \mathbf{q}) &= \left(B + 3B'(\text{tr } \boldsymbol{\epsilon})^2 + \mu + 2\mu'|\tilde{\boldsymbol{\epsilon}}|^2 + 8\mu'(\tilde{\boldsymbol{\epsilon}}\mathbf{q} \cdot \mathbf{q})^2\right)\mathbf{q} \otimes \mathbf{q} \\ &\quad + \left(\mu + 2\mu'|\tilde{\boldsymbol{\epsilon}}|^2 + 8\mu'(\tilde{\boldsymbol{\epsilon}}\mathbf{q} \cdot \mathbf{q}_\perp)^2\right)\mathbf{q}_\perp \otimes \mathbf{q}_\perp. \end{aligned} \quad (9)$$

The elastic spinodal is defined as the boundary of the region in the strain space, where the acoustic tensor is positive definite. In other words, on the *elastic spinodal*, one of the eigenvalues of $\mathbf{Q}(\boldsymbol{\epsilon}; \mathbf{q})$ becomes zero while the other may remain positive. Vanishing of the eigenvalue associated with the longitudinal modes $\mathbf{q} \otimes \mathbf{q}$ gives the aether-like threshold

$$B + 3B'(\text{tr } \boldsymbol{\epsilon})^2 + \mu + 2\mu'|\tilde{\boldsymbol{\epsilon}}|^2 + 8\mu'(\tilde{\boldsymbol{\epsilon}}\mathbf{q} \cdot \mathbf{q})^2 = 0, \quad (10)$$

while vanishing of the eigenvalue associated with the transverse/shear modes $\mathbf{q}_\perp \otimes \mathbf{q}_\perp$ gives the fluid-like threshold

$$\mu + 2\mu'|\tilde{\boldsymbol{\epsilon}}|^2 + 8\mu'(\tilde{\boldsymbol{\epsilon}}\mathbf{q} \cdot \mathbf{q}_\perp)^2 = 0. \quad (11)$$

If we diagonalize the strain tensor using the same Fourier basis $\boldsymbol{\epsilon} = \epsilon_1\mathbf{q} \otimes \mathbf{q} + \epsilon_2\mathbf{q}_\perp \otimes \mathbf{q}_\perp$, equations (10) and (11) reduce, respectively, to the following equations for elastic spinodals in the space of principal strains:

$$B + \mu + 3B'(\epsilon_1 + \epsilon_2)^2 + 3\mu'(\epsilon_1 - \epsilon_2)^2 = 0, \quad (12a)$$

$$\mu + \mu'(\epsilon_1 - \epsilon_2)^2 = 0. \quad (12b)$$

3. THE STOCHASTIC MODEL

To develop an adiabatic approximation, consider first the potential $G(x, z) = (|x| - k_0)^2/2 + (x - z)^2/2 - xA$ with fixed bias A . This means that at the time scale of the barrier crossing we assume that the driving force is constant $f(t) \equiv A$. Then the solution of the time independent Fokker-Planck equation $0 = \partial_x [p\partial_x G + D\partial_x p]$ can be obtained explicitly $p_A(x) = Z^{-1}e^{-G(x,z)/D}$, with $Z = \int_{-\infty}^{\infty} e^{-G(x,z)/D} dx$. Under such an assumption of time scale separation, the time-averaged probability distribution for the periodic driving introduced in the main paper can be written as $p_{\text{ad}}(x) = (p_A(x) + p_{-A}(x))/2$. To compute the corresponding integrals we need to use the formula

$$\begin{aligned} &\int e^{-[c_1(x-a)^2 + c_2(x-b)^2 - c_3x]} dx \quad (13) \\ &= \frac{1}{2} \sqrt{\frac{\pi}{c_1 + c_2}} e^{-\frac{4(a-b)^2 c_1 c_2 - 4(c_1 a + c_2 b)c_2 - c_3^2}{4(c_1 + c_2)}} \\ &\times \text{erf}\left(\frac{2(c_1 + c_2)x - 2(c_1 a + c_2 b) - c_3}{2\sqrt{c_1 + c_2}}\right) \end{aligned}$$

which is easily checked by completing the square. Using (14), with $c_1 = \frac{1}{2D}$, $c_2 = \frac{k}{2D}$, $c_3 = \frac{A}{D}$, $a = \pm k_0$ and $b = z$, we obtain an analytical expression for the effective force $T(z) = k(z - \langle\langle x \rangle\rangle)$ ($\langle\langle \cdot \rangle\rangle$ is the average over ensemble and time) which we do not present here as it is rather

cumbersome. In the main text we performed numerical computation of the remaining integrals and obtain the effective elastic spring potential $F(z)$, shown in Fig. 6 in the main text.

[1] H. C. Simpson and S. J. Spector, *On the failure of the complementing condition and non-uniqueness in linear elastostatics*, *Journal of Elasticity* **15**, 229-231 (1985).

[2] M. Šilhavý, *The Mechanics and Thermodynamics of Continuous Media*, Springer-Verlag (1997).